Editorial manuscript ref. no:

# Effect of temperature-dependent air properties on the accuracy of numerical simulations of thermal airflows over pinned heat sinks

**Amer Al-Damook[1,2], J.L. Summers[1], N. Kapur[1], H. Thompson[1]**

[1]School of Mechanical Engineering, University of Leeds, UK

[2]Mechanical Engineering Department, University of Anbar, MOHESR, HCED, Iraq

## Abstract

The importance of accounting for the temperature-dependence of air properties in numerical simulations of air flows over pinned heat sinks is demonstrated by comparisons with recently published experiments. Numerical simulations, based on a conjugate heat transfer analysis, using the RANS-based modified k-ω turbulence model, with temperature-dependent air properties are shown to be in significantly better agreement with experimental measurements of pressure drop, heat transfer coefficient and heat sink base temperature, than those which employ constant air properties.

**Keywords**: temperature-dependent air properties, conjugate heat transfer, turbulent airflow, pinned heat sink.

*Corresponding author:

Email:mansj@leeds.ac.uk

## Nomenclatures

| | | | |
|---|---|---|---|
| $A_c$ | cross-sectional area of the flow passage of the heat sink, $m^2$ | Re | Reynolds number |
| D | pin diameter of the pin fin heat sink, mm | T | temperature, $^oC$ |
| d | perforation diameter of the pin fin, mm | $T_{base}$ | Base temperature, $^0C$ |
| $D_h$ | hydraulic diameter, m | $\Delta T$ | temperature difference, $^oC$ |
| H | pin fin height, mm | U | air velocity, m/s |
| H | heat transfer coefficient, $W/m^2.K$ | **Greek** | |
| k | turbulence kinetic energy, $m^2s^{-2}$ | $\alpha$ | fluid thermal diffusivity, $m^2/s$ |
| n | number of perforations | $\alpha,\beta,\beta^*$ | turbulence model constant |
| N | number of pins | $\mu$ | fluid viscosity, Pa·s |
| L | heat sink length, mm | $\mu_t$ | turbulent eddy viscosity, Pa.s |
| Nu | Nusselt number | $P$ | fluid density, $kg/m^3$ |
| $P_{fan}$ | fan power, W | $N$ | kinematic viscosity, $m^2/s$ |
| $\Delta P$ | pressure drop, Pa | $\nu_t$ | turbulent kinematic viscosity, $m^2/s$ |
| Pr | Prandtl number | $\sigma_\varepsilon$ | k-ε turbulence model constant |
| $Pr_t$ | turbulent Prandtl number | $\sigma$ | turbulence model constant for the k-equation |
| Q | power applied on the base, W | $\omega$ | k-ω turbulence model constant |
| $S_z$ | pin pitch in streamwise direction, mm | | |

## 1. INTRODUCTION

Rising heat flux densities are presenting the micro-electronics industry with a number of formidable challenges in providing adequate cooling to avoid thermally-induced failure modes [1]. This paper considers the most popular approach to micro-electronics cooling, recently shown to account for more than 80% of its thermal management solutions, namely convective heat transfer to air as it flows over a network of extended surface fins on a heat sink [2]. Although plate fin heat sinks (PFHSs) are the most common heat sink designs [3], a number of recent studies have demonstrated the benefits of employing strip [4], and pin fins are more effective turbulence promoters which break up the thermal boundary layer that would otherwise form over the heat sink [5] and [6].

These studies have also shown that perforating the fins in heat sinks can offer substantial performance benefits for micro-electronics cooling, enabling lower processor temperatures to be achieved with less mechanical power consumption. Al-Damook et al [7], for example, used complementary experimental and numerical methods to explore the benefits of using multiple pin perforations in pinned heat sinks (PHSs) and Al-Damook et al [8] have reported the benefits of optimum rectangular slotted and notched pin perforations, while Al-Sallami et al [4] extended this work to consider the benefits of multiple perforations and fin arrangement for heat sinks with strip fins. However, as in previous numerical simulations of thermal air flows over heat sinks, both studies ignored the variation in air flow properties that inevitably results from the temperature variation across heat sinks and proposed that the discrepancies of up to 15% that they found between their experimental measurements and numerical predictions may be due to the practical difficulties of achieving exact perforation alignment and additional thermal resistance and surface roughness induced during the manufacturing process.

This paper demonstrates that the discrepancies between experiment and theory for thermal airflows over heat sinks can be reduced significantly by accounting for temperature-dependent air properties in the numerical simulations. The paper is organised as follows. Section 2 describes the conjugate heat transfer model for the thermal airflows past the PHS under consideration and the numerical methods to solve them. Numerical solutions for with and without temperature-dependent air properties are compared with the recently-published experimental data of Al-Damook et al [7] in Section 3 and conclusions are drawn in Section 4.

## 2. NUMERICAL METHODS

### 2.1 Geometry description and governing equations

The aluminium PHS configurations considered here are those studied experimentally by Al-Damook et al [7], with base dimensions 50mm x 50mm x 2mm an array of equally spaced pins (with 6.5mm separation in the longitudinal and transverse directions) of circular cross-section of diameter and height 2mm and 10mm respectively. Thermal airflows past PHS configurations with solid pins (0P) and perforated pins (3P), as defined in Figure 1, are considered.

A conjugate heat transfer model is used, where the thermal airflow through the PHS is analysed using Computational Fluid Dynamics (CFD). The inlet air temperature is set to 18$^{o}$C and the inlet air velocity is varied between 6.5m/s and 12m/s leading to Reynolds numbers in the range 3500-6580 based on a length scale given by the hydraulic diameter of the duct $D_h$=2H.B/(H+B), where H and B are height and width of duct in which the heat sink is located, respectively. The rate of heat conduction through the aluminium heat sink is balanced by heat transfer by convection into the moving air stream, through a coupled boundary condition at the solid/fluid interface, as illustrated in Figure 2.

In the solid heat sink the temperature field $T_s$ is obtained by solving the steady heat conduction equation

$$\nabla.(k_s \nabla T_s) = 0 \qquad (1)$$

where $k_s$=202W/m.K is the thermal conductivity of the aluminium heat sink. Turbulent airflow through the PHSs is modelled using Reynolds-Averaged Navier-Stokes (RANS) equations, Zhou & Catton [9], where the continuity, momentum and energy equations have variables decomposed into mean and fluctuating components, leading to:

$$\frac{\partial \rho}{\partial t} + \nabla.\rho \underline{U} = 0 \qquad (2)$$

$$\frac{\partial (\rho \underline{U})}{\partial t} + \nabla.(\rho \underline{U})\underline{U} = \nabla.\left(\underline{\underline{\sigma}} - \rho \overline{\underline{U}'}\,\overline{\underline{U}'}\right) \qquad (3)$$

where $\underline{\underline{\sigma}} = -p\underline{\underline{I}} + \mu\left(\nabla \underline{U} + [\nabla \underline{U}]^T\right)$ and $-\rho \overline{\underline{U}'}\,\overline{\underline{U}'} = \mu_t \left(\nabla \underline{U} + [\nabla \underline{U}]^T\right) - 2/3(\rho k \underline{\underline{I}})$ are the Newtonian and Reynolds Stress tensors respectively, $\mu$ is the air viscosity, $\rho$ its density, $\underline{U}$ and $\overline{\underline{U}'}$ the average and turbulent fluctuation velocity vectors respectively, p is the pressure and $\underline{\underline{I}}$ the unit

tensor. The RANS equations are solved with the energy equation for the temperature field in the fluid, $T_f$, with a heat source $\dot{Q}$ Watts, using the following equation

$$\rho \frac{\partial C_p T_f}{\partial t} + \rho \underline{U}.\nabla(C_p T_f) = \nabla\left(k + \frac{C_p \mu_t}{Pr_t}\right)\nabla T_f + \dot{Q} \quad (4)$$

where $C_p$ is the specific heat capacity of the air, Pr and $v$ are the Prandtl number and kinematic viscosity of the air respectively and the subscript t indicates their turbulent counterparts.

Following Al-Damook et al [7] and Zhou & Catton [9] the thermal airflow through the heat sink is modelled using the k-$\omega$ SST model and the effects of radiative heat transfer are neglected. The equations for the SST model are not reproduced here for reasons of brevity.

### 2.2 Computational domain and boundary conditions

The computational problem is reduced in size by exploiting the symmetry of the PHS to apply symmetry boundary conditions along the sides of the channel (Figure 3). This domain should be far enough at the entrance and exit regions of heat sinks to avoid any reverse flow and the side effects of boundaries. Therefore, the entrance and exit regions are a distance of 12.5d away from the heat sink in the X-direction of flow.

The fluid and thermal conditions are assumed to be:

1- At inlet airflow: 6.5m/s ≤ $U_{air}$ ≤ 12m/s, and the inlet air temperature: $T_{in}$=18$^o$C.

2- Interface solid-fluid surfaces (pinned heat sink): no-slip condition $U_{in}$=0m/s, and heat flux is conserved $k_f.\frac{dT_f}{dn} = k_s.\frac{dT_s}{dn}$

3- At the bottom base wall of heat sinks: no-slip condition $U_{air}$=0m/s, and a uniform heat flux of Q=20000W/m$^2$.

4- At the outlet pressure airflow: P=$P_{gage}$=0Pa, $\frac{dT}{dx} = 0$

5- Top wall and other surfaces: $U_{air}$=0m/s, $\frac{dT}{dz} = 0$

6- Right and left sides: Symmetry surfaces $\frac{du}{dy} = 0$, $\frac{dT}{dy} = 0$

### 2.3 Solution Methods and Convergence Criteria

The finite volume method-based code, ANSYS FLUENT [10] is used to solve the fully coupled momentum and energy equations, using second order upwinding, while continuity is satisfied using the SIMPLE method. The grid is composed of tetrahedral mesh elements to improve the

quality of the numerical prediction near curved pin surfaces. Computation is started first by solving the continuity, momentum, k and $\omega$ equations to determine the flow field and then the energy equation to find the thermal field in the computational region. The procedure continues until the sum of the residuals of continuity and momentum equations in each cell is less than $10^{-4}$ and for energy equation is taken smaller than $10^{-6}$. The variation of viscosity ($\mu$), density ($\rho$), thermal conductivity (k), and thermal capacity ($C_p$) with temperature is accounted for using the data from Çengel et al [11] shows in Table 1. The CFD model accounts for their variation by calculating their values at specific temperatures by linear interpolation between the data points in Table 1.

## 3. Results and Discussion

The conjugate heat transfer model used here has been validated previously against a range of experimental and numerical data, see Al-Damook et al [7], [8] and [12]. A brief set of results is now presented which demonstrate the benefits of incorporating temperature-dependent viscosity ($\mu$), density ($\rho$), thermal conductivity (k), and thermal capacity ($C_p$) into numerical simulations of thermal airflows over heat sinks. Inlet air velocities are varied from 6.5m/s to 12m/s for the range of Reynolds number is 3500-6580. Numerical results are presented for both constant thermo-physical properties evaluated at 18$^o$C (Num.) and variable thermo-physical properties (Num. Variable), where the air properties $\mu$, $\rho$, k, and $C_p$ are approximated by linear interpolation from the data presented in Table 1. These are compared against the experimental data of Al-Damook et al [7] for PHSs with solid (0P) pins and pins with three circular perforations (3P).

### 3.1 Effect of variable air properties on pressure drop

Mechanical energy is required to overcome the pressure drop, $\Delta$P, that results from flow over a heat sink. It is therefore important to reduce $\Delta$P and the associated fan power required to overcome the pressure drop, $P_{fan}=U.A_c.\Delta P$, where U is the inlet air velocity and $A_c$ is the cross-sectional area of the flow passage of the heat sink=$H.S_z.(N-1)$, where $S_z$ is the uniform pin spacing. Figure 5(a) compares predictions of $\Delta$P against the experimental data. Note that the use of perforated pins results in reductions in $\Delta$P of up to 9%, Al-Damook et al [7]. For the solid and perforated pins, the pressure drops predicted using constant air properties are typically 10% lower than the experimental data, whereas for predictions using variable air properties the error has halved to around 5%. It is likely that this improvement is due to the increase in viscosity as the air temperature raises that required higher pressure drop to push the air through the heat sink. Figure 5(b) shows the effect that this improvement has on predictions of the fan power consumption, $P_{fan}$.

### 3.2 Effect of variable air properties on heat transfer

Figure 6 compares experimental measurements of Nusselt number, Nu and CPU temperature $T_{case}$, for heat sinks with the 0P and 3P pin designs against numerical calculations using either constant or variable air properties. Nusselt number is defined by $Nu = h.L/k_{air}$, in terms of the heat transfer coefficient, h ($W/m^2K$), the length of the heat sink in the flow direction , L (m), and $k_{air}$ (W/mK), the thermal conductivity of the air. The heat transfer coefficient is defined by $h = \frac{\dot{Q}}{A_T(T_s - T_m)}$, where $A_T$ is the total surface area including the pin and perforation surface areas ($m^2$), $T_s$ is the heat sink pin surface temperature and $T_m$ is the average bulk mean temperature $T_m=(T_{in}+T_{out})/2$.

Figure 6 presents the corresponding experimental measurements and numerical predictions of Nusselt number. The data shows that both Nu increases approximately linearly with the inlet air velocity and that the 3P pin fins design achieves a significant enhancement in heat transfer. The experimental values of Nu is typically 10% smaller than those predicted numerically with constant air properties, whereas for those with variable air properties, discrepancy is reduced to 5%.

Figure 8 compare experimental measurements and numerical predictions for the CPU temperature, $T_{case}$. Since the experimental heat transfer coefficients are lower than the predictions, it follows that the experimental $T_{case}$ values will be larger. Experimental $T_{case}$ values for a heat sink with the perforated 3P pins are typically around 6% smaller than for solid pin fins. The error numerical predictions of $T_{case}$ with constant thermo-physical properties is nearly 3% and 5% for 0P and 3P heat sink models respectively, while with variable thermo-physical properties are typically 2% and 4% for 0P and 3P heat sink models respectively (1.5$^o$C larger) and therefore closer to the experimental results than with constant air properties.

## 4. Conclusion

This paper is the first to quantify the benefits of accounting for thermal variations of air properties on the accuracy of numerical predictions of thermal airflows over heat sinks. It has shown that the discrepancies between the experimental and the numerical prediction with constant air properties of up to 15% can be reduced to between 5-10% when variable air properties are incorporated into numerical simulations, as shown on Table 2. It is likely that the main factor that should be accounted for is the air viscosity which rises significantly with temperature, causing increased pressure losses and reduced heat transfer over the heat sink, in line with the recent experimental data of Al-Damook et al [7]. Based on this study, it is recommended that the variable air properties should be accounted for in future heat sink thermal air flow simulations.

## 5. Acknowledgements

The authors would like to thank the Higher Committee for Education Development in Iraq (HCED), Iraqi Ministry of Higher Education and Scientific Research (MOHE), and Mechanical Engineering Department University of Anbar, Iraq for financial support of this work (Amer Al-Damook: D2-87-2334).

**References**


1. S. Gurrum, S. Suman, Y. Joshi and A. Fedorov, "Thermal Issues in Next-Generation Integrated Circuits", IEEE Transactions on Device and Materials Reliability, vol. 4, no. 4, pp. 709-714, 2004.
2. A. McWilliams, "The Market for Thermal Management Technologies - SMC024G", Bccresearch.com, 2015. [Online]. Available: http://www.bccresearch.com/market-research/semiconductor-manufacturing/thermal-management-technologies-market-smc024g.html. [Accessed: 22- Dec- 2015].
3. M. Shaeri and M. Yaghoubi, "Numerical analysis of turbulent convection heat transfer from an array of perforated fins", International Journal of Heat and Fluid Flow, vol. 30, no. 2, pp. 218-228, 2009.
4. W. Al-Sallami, A. Al-Damook, H.M. Thompson, 'A Numerical Investigation of Thermal Airflows over Strip Fin Heat Sinks, International Communications in Heat and Mass Transfer, **75**, 183-191, 2016.
5. B. Sahin and A. Demir, "Thermal performance analysis and optimum design parameters of heat exchanger having perforated pin fins", Energy Conversion and Management, vol. 49, no. 6, pp. 1684-1695, 2008.
6. B. Sahin and A. Demir, "Performance analysis of a heat exchanger having perforated square fins", Applied Thermal Engineering, vol. 28, no. 5-6, pp. 621-632, 2008.
7. A. Al-Damook, N. Kapur, J. Summers and H. Thompson, "An experimental and computational investigation of thermal air flows through perforated pin heat sinks", Applied Thermal Engineering, vol. 89, pp. 365-376, 2015.
8. A. Al-Damook, N. Kapur, J. Summers and H. Thompson, Computational Design and Optimisation of Pin Fin Heat Sinks with Rectangular Perforations, Applied Thermal Engineering Journal, 2016
9. F. Zhou and I. Catton, "Numerical Evaluation of Flow and Heat Transfer in Plate-Pin Fin Heat Sinks with Various Pin Cross-Sections", Numerical Heat Transfer, Part A: Applications, vol. 60, no. 2, pp. 107-128, 2011.
10. ANSYS FLUENT User's Guide, 2011
11. Y.A. Çengel, and M. John Cimbala. Fluid Mechanics: Fundamentals and Applications. Boston: McGraw-HillHigher Education, 2006.

12. A. Al-Damook, N. Kapur, J. Summers and H. Thompson, Effect of Different Perforations Shapes on the Thermal-hydraulic Performance of Perforated Pinned Heat Sinks. Journal of Multidisciplinary Engineering Science and Technology, vol.3, no. 4, pp. 4466-4474, 2016.

**Table Captions**

**Table 1** : The variation air properties with increasing air temperature.

**Table 2:** The errors percentage between the experimental and numerical data at constant and variable air properties.

**Table 3** : The variation air properties with increasing air temperature.

| Air temperature ($^oC$) | Dynamic Viscosity (kg/m.s) | Density ($kg/m^3$) | Thermal Conductivity (W/m.K) | Specific Heat (J/kg.K) |
|---|---|---|---|---|
| 15 | $1.802 \times 10^5$ | 1.225 | 0.02476 | 1007 |
| 25 | $1.849 \times 10^5$ | 1.184 | 0.02551 | 1007 |
| 45 | $1.941 \times 10^5$ | 1.109 | 0.02699 | 1007 |
| 60 | $2.008 \times 10^5$ | 1.059 | 0.02808 | 1007 |
| 80 | $2.096 \times 10^5$ | 0.9994 | 0.02953 | 1008 |
| 100 | $2.181 \times 10^5$ | 0.9458 | 0.03095 | 1009 |
| 120 | $2.264 \times 10^5$ | 0.8977 | 0.03235 | 1011 |

**Table 4:** The errors percentage between the experimental and numerical data at constant and variable air properties.

| Type of properties | $\Delta P$ (Pa) | $Nu_T$ | $T_{case}$ ($^oC$) | |
|---|---|---|---|---|
| Constant air properties | 10% | 10% | 0P | 3P |
| | | | 3% | 5% |
| Variable air properties | 5% | 5% | 0P | 3P |
| | | | 2% | 4% |

**Figure captions**

**Figure 1:** Solid (0P) and perforated (3P) perforations considered [7].

**Figure 2:** Conjugate heat transfer model for the PHS [7].

**Figure 3:** Schematic diagram of the flow domain used in the CFD analyses, shown eight perforated pin fins [12].

**Figure 4:** Effect of pin perforations on (A) pressure drop and (B) fan power as a function function of airflow speed..

**Figure 5:** Effect of inlet velocity on Nusselt number based on total surface area.

**Figure 6:** Comparison between experimental and numerical predictions of influence of fan power on $T_{case}$.

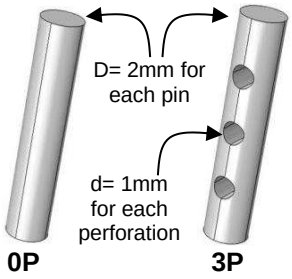


**Figure 1:** Solid (0P) and perforated (3P) perforations considered [7].

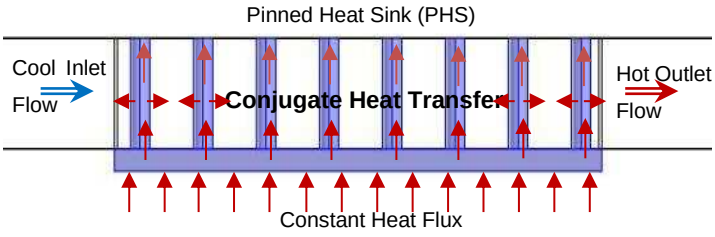


**Figure 2:** Conjugate heat transfer model for the PHS [7].

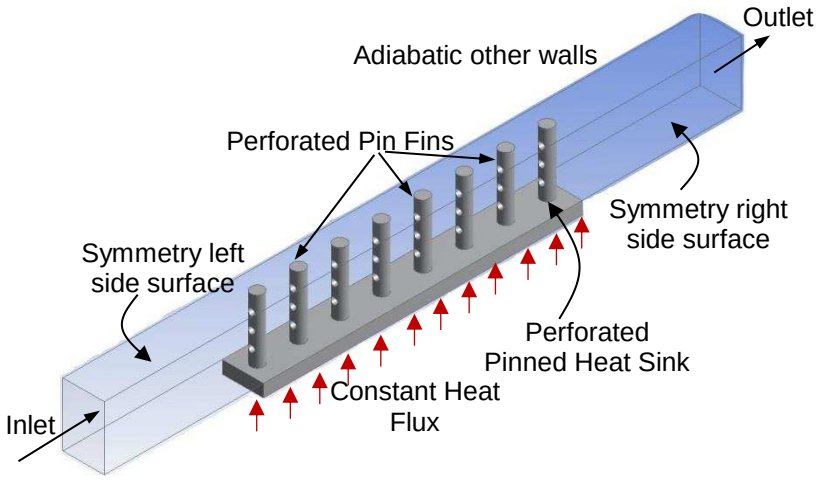


**Figure 3:** Schematic diagram of the flow domain used in the CFD analyses, shown eight perforated pin fins [12].

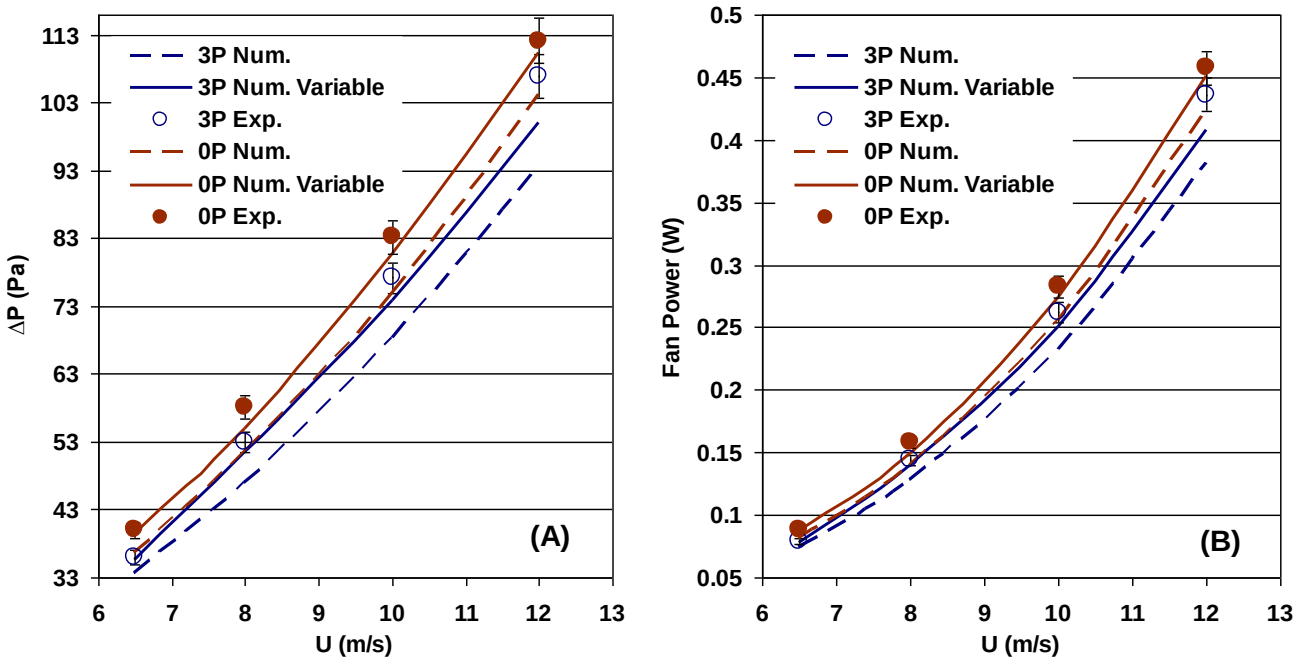


**Figure 4:** Effect of pin perforations on (A) pressure drop and (B) fan power as a function of airflow speed.

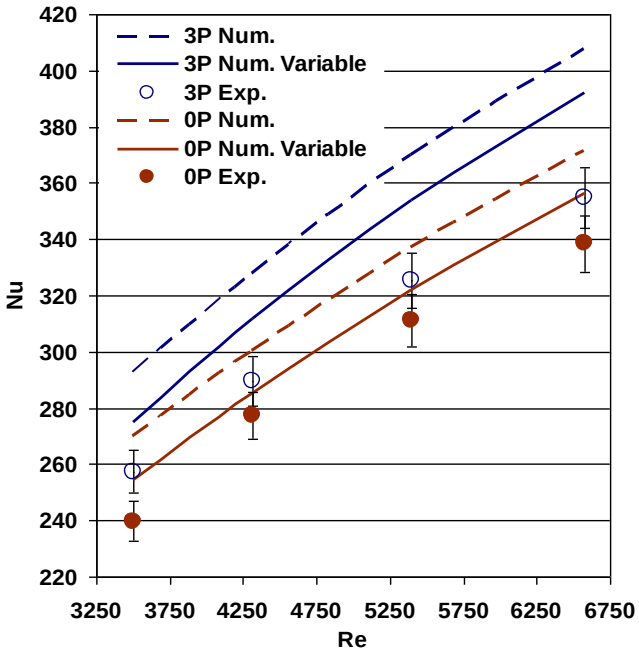


**Figure 5:** Effect of inlet velocity on Nusselt number based on total surface area.

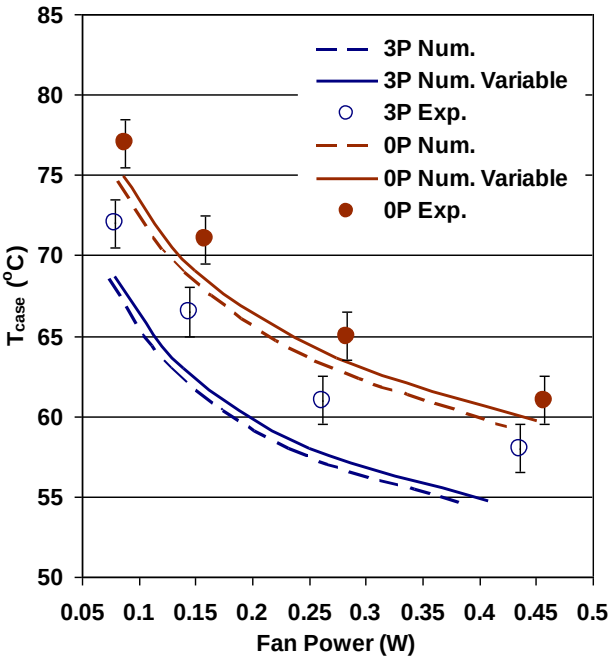


**Figure 6:** Comparison between experimental and numerical predictions of influence of fan power on $T_{case}$.